Contents lists available at ScienceDirect

Transactions of Nonferrous Metals Society of China

36(2026) 614−627

www.tnmsc.cn

# Petrogenesis of Early Mesozoic Furong pluton in central Hunan, China and its implications for tungsten mineralization

Jian-xiong DU [a], Jian-tang PENG [b,*], A-xiang HU [b,c,**], Ta-gen DAI [d], Meng-ying SUO [b], Li-chao XIAHOU [d]

[a] School of Management Science and Engineering, Guizhou University of Finance and Economics, Guiyang 550025, China;

[b] State Key Laboratory of Critical Mineral Research and Exploration, Institute of Geochemistry, Chinese Academy of Sciences, Guiyang 550081, China;

[c] College of Civil Engineering, Hunan City University, Yiyang 413000, China;

[d] School of Geosciences and Info-physics, Central South University, Changsha 410083, China

**Abstract:** The Furong pluton, located in central Hunan, China, hosts numerous tungsten veins within and around the granite, which are of great economic significance. However, its petrogenesis and related mineralization are poorly constrained. In this study, we used U−Pb dating, petrological and geochemical methods to ascertain the emplacement time, classification of granitic rock, nature of the source rocks, formation mechanism, and its geodynamic implications for the Furong pluton. It is shown that the granite is precisely determined to be formed at ~210 Ma, and belongs to the moderately-fractionated S-type granite. Combined with regional tectonic setting, it is concluded that the pluton was formed due to crust extension and thinning followed by plate collision and compression in South China. It is also revealed that tungsten mineralization and Indosinian granites exhibit a close temporal, spatial and genetic relationships, and further exploration of tungsten deposits within and around the granite in central Hunan, even in South China, is urgently needed.
**Keywords:** zircon U−Pb dating; Indosinian; tungsten mineralization; Furong pluton; South China

## 1 Introduction

Mesozoic granites are widely distributed in South China [1−3], and previous researches have mostly focused on the Late Mesozoic (Yanshanian) granite and its related mineralization during the past several decades [4−7]. In contrast, the Early Mesozoic (Indosinian) granite and its relevant mineralization have been ignored for a long time due to their relatively limited outcrop area [2,8,9]. In recent years, many researchers have proposed that Indosinian magmatism is relatively widespread in South China [10−13]; however, up to now, the affected scope and the intensity of the Indosinian magmatic activity have been seriously underestimated [14], and its mineralization potential has received less attention.

The Early Mesozoic granite mainly exhibits a planar distribution in Hunan, Jiangxi, Guangdong, Guangxi, and Fujian Provinces in South China [2,14], with a small quantity and scattered distribution [14,15]. Among them, the Xiangzhong area (central Hunan, China) is the most important distribution region, and many tungsten (W) mineralizations related to these granites occur in this area. The important tungsten deposits and their associated granites include the Xingfengshan Au−W deposit and the adjacent Baimashan pluton, the Baojinshan Au−W deposit and the adjacent Ziyunshan pluton,

**Corresponding author:** *Jian-tang PENG, Tel: +86-851-85895405, E-mail: jtpeng@126.com;
**A-xiang HU, Tel: +86-15973114149, E-mail: axhu2010@163.com
https://doi.org/10.1016/S1003-6326(25)66985-8
Received 29 November 2024; accepted 16 September 2025

the Darongxi W deposit and the adjacent Dashenshan pluton, the Muguayuan W deposit and the adjacent Sanxianba pluton, and the Situpu W deposit and the adjacent Weishan pluton (Fig. 1 [16]). Although some petrological and geochemical researches have been carried out on these Early Mesozoic granites in central Hunan, China in recent years [8,9,14], it is still unclear whether there are multiple episodes of granitic magma emplacement during the Early Mesozoic, the nature of its magma source is still ambiguous, and the associations between the granites and tungsten mineralization are still disputed.

The Furong pluton, adjacent to the Weishan pluton, was considered to be formed during the Mesozoic, but robust geochronological constraints on its emplacement are still absent. Many tungsten-bearing quartz veins occur within this pluton and some occur along the contact zone between the granite and the Neoproterozoic slate, forming a medium-scale tungsten deposit [17]. Unfortunately, the geological and geochemical features of the Furong pluton are poorly constrained, and the relationship between the pluton and the tungsten mineralization is still ambiguous. Moreover, it is unclear whether the Furong pluton is a part of the adjacent Weishan pluton. The above problems seriously restrict our understanding of the petrogenesis of the Furong pluton and the relevant tungsten mineralization. Numerous tungsten-bearing veins develop inside and around the Furong pluton, and are of great economic significance; however, the petrogenesis of the pluton and its related mineralization are poorly constrained.

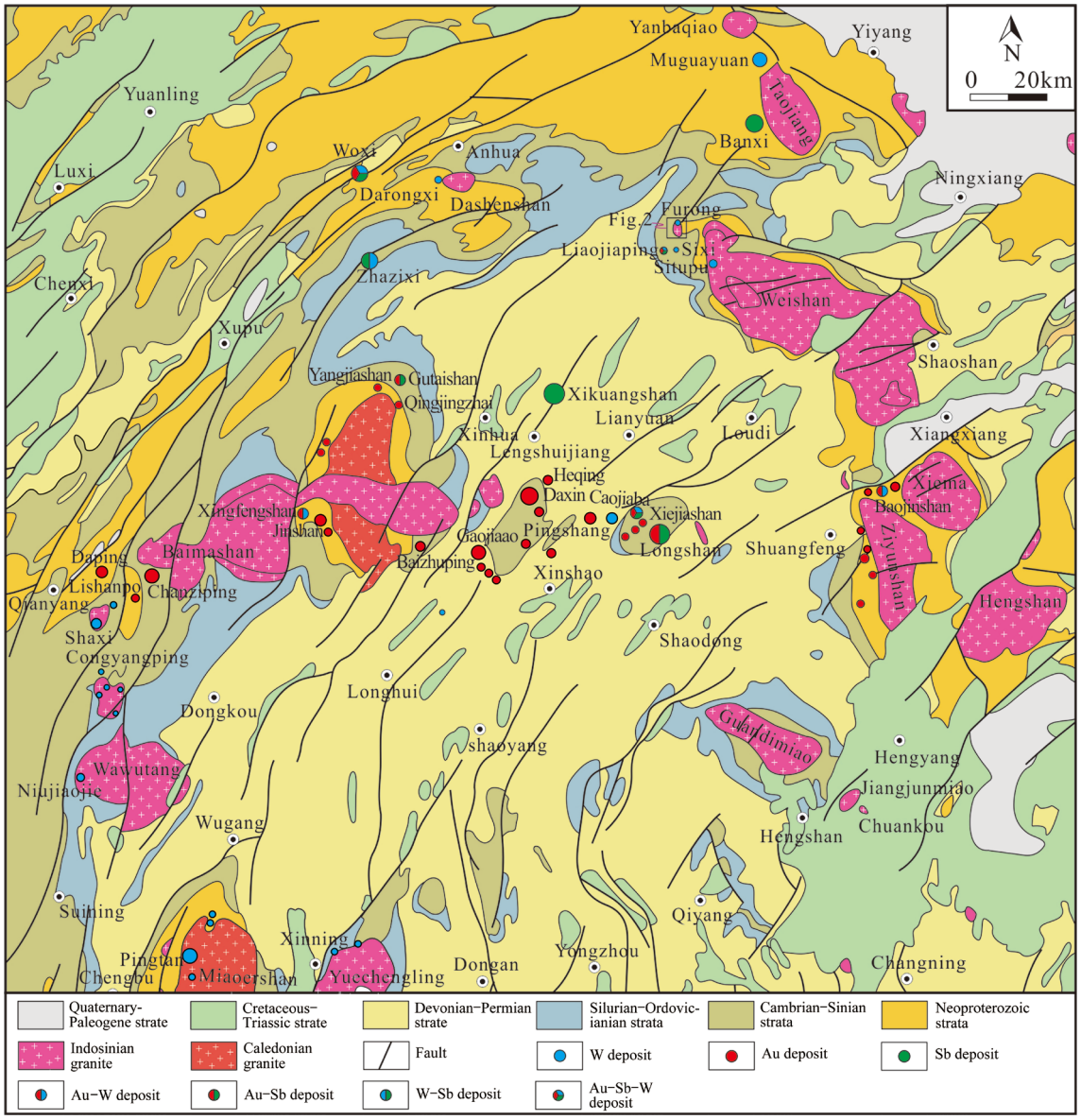


**Fig. 1** Regional geological map of central Hunan, South China (Modified from Ref. [16])

In this study, based on the geological and geochemical signatures of Furong pluton, we determined the rock type, magma source, and geodynamic setting of the pluton for the first time. We also measured the emplacement time of Furong pluton, and investigated the relationship between the granite emplacement and tungsten mineralization during the Early Mesozoic in central Hunan, South China. These conclusions achieved in this study will promote the further understandings regarding the Early Mesozoic granites and its related mineralization throughout South China, and provide theoretical guidance for the exploration of tungsten mineralization within or around the granitic pluton.

## 2 Geological setting and analytical methods

The Xiangzhong Metallogenic Province is located in the central part of the Jiangnan Orogen. This orogen is situated between the Yangtze and Cathaysia blocks, provides a key to understanding the crustal evolution, magmatic activity and metallogenic effects in South China [18]. The Proterozoic basement outcropped in central Hunan is mainly composed of the Banxi Group ($Pt_3b$) and Lengjiaxi Group ($Pt_3ln$), and consists of low-grade greenschist facies metamorphic rocks. The magmatic activity in this region is intense and frequent, and can be mainly divided into Indosinian and Caledonian magmatisms [12,14]. A series of Indosinian granites have intruded into the Proterozoic and Early Paleozoic strata around the Xiangzhong Basin (Fig. 1), and some tungsten deposits related to these granites have been newly discovered in recent years [12,17,19,20].

The Furong pluton is located in Anhua County (Hunan Province, China), approximately 6 km east away from the Weishan pluton (Fig. 1). The Furong pluton exhibits an irregular elliptical shape, about 4.4 km in north-south length, and 1.7 km in east-west width, with an exposed area of 6 $km^2$. Tectonically, the studied area is located in the middle part of the arc-shaped Xuefengshan structural belt. The exposed strata include the Wuqiangxi Formation of the Neoproterozoic Banxi Group ($Pt_3bnw$), and the Jiangkou Formation ($Z_1j$), Xiangmeng Formation ($Z_1x$) and Hongjiang Formation ($Z_1h$) of the Lower Sinian (Fig. 2 [17]). Structures are well developed in this area, including NE-trending and EW-trending faults, the Furong complex anticline and its secondary folds (Fig. 2).

Tungsten mineralization predominantly occurs in the form of scheelite–quartz veins within the granitic pluton, and some ore veins are distributed in the outer contact zone (Fig. 2). Ore veins in the Furong deposit are morphologically simple, mostly occurring in the form individual veins or lenses. Among all ore veins, No. I vein is the largest in scale, with a length of more than 1300 m and a thickness of 0.6−5.5 m [17]. Scheelite is the sole ore mineral, with pyrite occurring locally. The gangue minerals are predominantly quartz, with small amounts of muscovite and sericite.

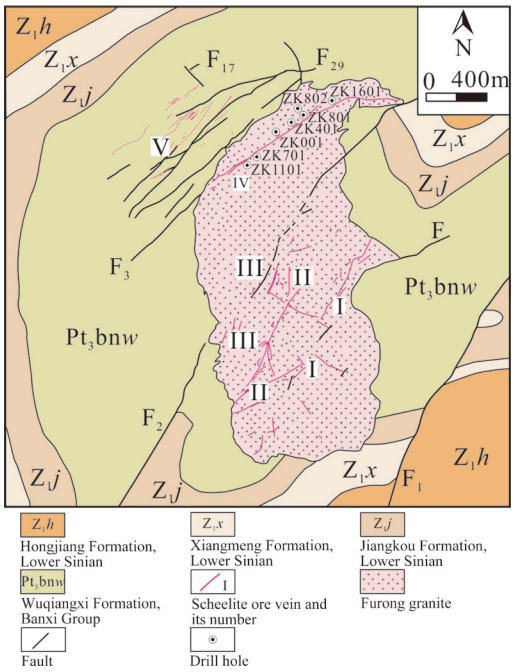


**Fig. 2** Geological map of Furong tungsten deposit in central Hunan, China (Modified from Ref. [17])

In this study, twenty samples were collected from five boreholes within the Furong pluton. The granite samples mainly consist of quartz (25−35 vol.%), K-feldspar (25−30 vol.%), plagioclase (30−40 vol.%), biotite (4−10 vol.%) and muscovite (0−5 vol.%), and are classified as monzonite granite (Fig. 3). Accessory minerals include apatite, zircon, tourmaline, garnet and ilmenite. Among them, ten fresh samples were selected for the whole-rock chemical analysis (major and trace elements, Sr and Nd isotopes), including FR-1, FR-3 and FR-4 from the borehole ZK401; FR-5, FR-6 and FR-8 from the borehole ZK001; FR-11 from the borehole ZK801; FR-14 and FR-16 from the borehole ZK802; FR-19 from the borehole ZK701.

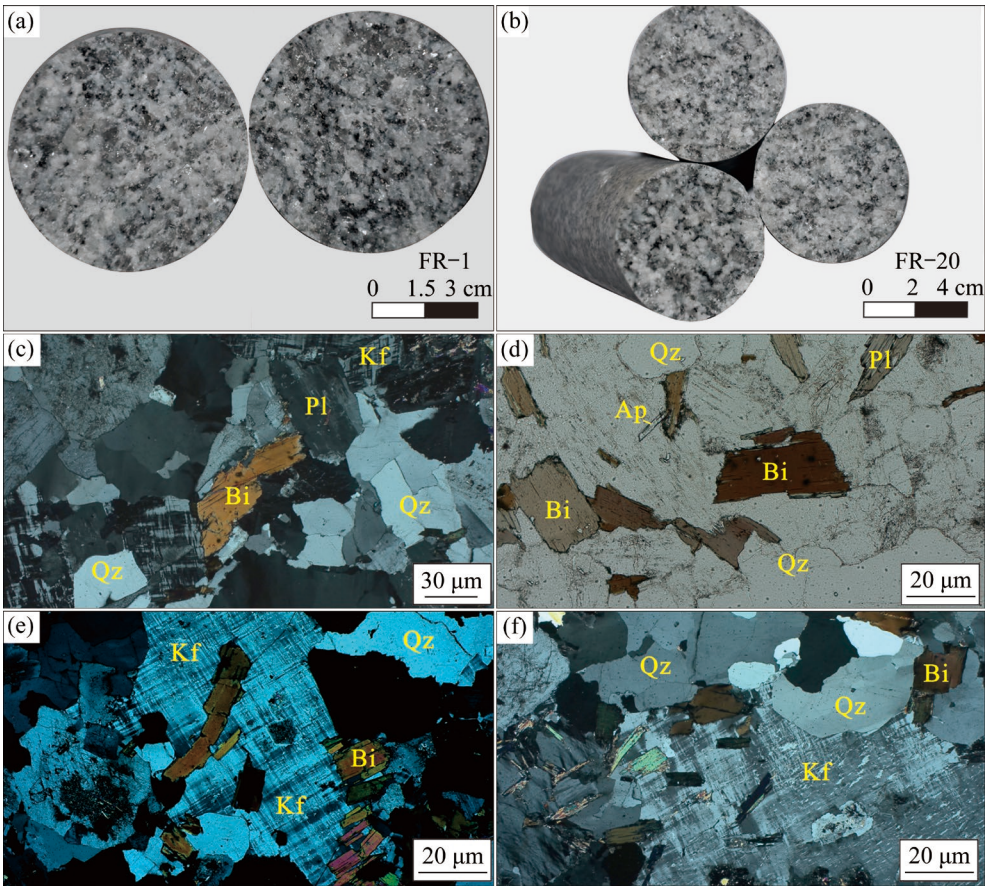


**Fig. 3** Photographs of representative hand-specimen (a, b) and micrographs (c−f) of granite collected from Furong pluton (Mineral abbreviations: Ap–Apatite; Bi–Biotite; Pl–Plagioclase; Qz–Quartz; Kf–K-feldspar)

Bulk analyses of major and trace elements, Rb−Sr and Sm−Nd isotopes were conducted at Guizhou Tongwei Analytical Technology Co., Ltd., China. The contents of major elements were determined using an ARL Perform'X 4200 instrument (Thermo Fisher). The trace element analysis was carried out via the inductively coupled plasma mass spectrometry (ICP–MS) (Thermo Fisher, X2). The standard samples utilized in this study were W-2a, BHVO-2, and BCR-2, and the analytical precision in this study was better than 5%. Sr and Nd isotopic ratios were measured using a Nu Instruments Plasma 3 multi-collector (MC)−ICP−MS. The analytical precision of the isotopes ratio in this study is reported as 2$\sigma$ standard errors.

Zircons selected from samples FR-3 and FR-19 were subjected to the laser ablation inductively coupled plasma mass spectrometry (LA−ICP−MS) U−Pb dating. After crushing, heavy liquid separation, and magnetic separation of the samples, cathodo-luminescence (CL) photography was performed. Zircon U−Pb dating was completed via the LA−ICP−MS, with a laser beam spot diameter of 30 μm, and the energy density and frequency were set to 10 J/cm$^2$ and 10 Hz, respectively. Zircon particle selection, target preparation, CL photography, zircon trace element analysis, and U−Pb isotopic analyses were all performed at Micro−Macro Geochemistry Technology (Langfang) Co., Ltd., China.

## 3 Results

### 3.1 Zircon U−Pb ages

The $w$(Ce) concentrations of zircon grains from the Furong pluton obtained in this study fall in (6−165)×10$^{-6}$ (mostly <50×10$^{-6}$), the Ce anomaly ($\delta_{Ce}$) and Eu anomaly ($\delta_{Eu}$) values vary in the range of 1.0−134.4 and 0.2−0.5, respectively, which are consistent with the values of those typical magmatic zircons. The mass fraction ratios of Th to U ($w$(Th)/$w$(U)) of the zircons in this study are 0.14−0.71 (>0.1), falling in the range of standard magmatic zircons [14].

Samples FR-3 and FR-19 in this study belong to the biotite monzogranite in term of lithology. Zircons from both samples display similar morphology and internal structures under CL, and most grains display well-developed crystal shapes and obvious rhythmic bands, indicating that they are of typical magmatic origin (Fig. 4).

For the zircon sample FR-3, the LA−ICP−MS analysis revealed that these zircon grains have highly variable mass fractions of U ($w$(U)=(484−5445)×10$^{-6}$), and the $w$(Th)/$w$(U) ratios fall in the range of 0.14−0.71, mostly clustering within 0.14−0.49. And 26 analytical points yield a $^{206}$Pb/$^{238}$U concordia age of (209.4±0.8) Ma (Fig. 4(a)). For sample FR-19, zircons grains display highly variable $w$(U) values of (442−5605)×10$^{-6}$, and the $w$(Th)/$w$(U) ratios change from 0.20 to 0.52, mostly clustering within 0.20−0.49. Most analytical points (28 of 30) define a concordia age of (210.7±0.8) Ma (Fig. 4(b)). All dates determined in this study are consistent within the error, indicating that the Furong pluton was emplaced at ~210 Ma.

### 3.2 Whole-rock geochemistry

The bulk analytical results of major elements for the Furong pluton are presented in Table 1. It is worthwhile to note that, the Weishan pluton shares similar lithological signatures with the Furong pluton, thus, both plutons are likely connected at greater depth, as previously speculated [21]. To

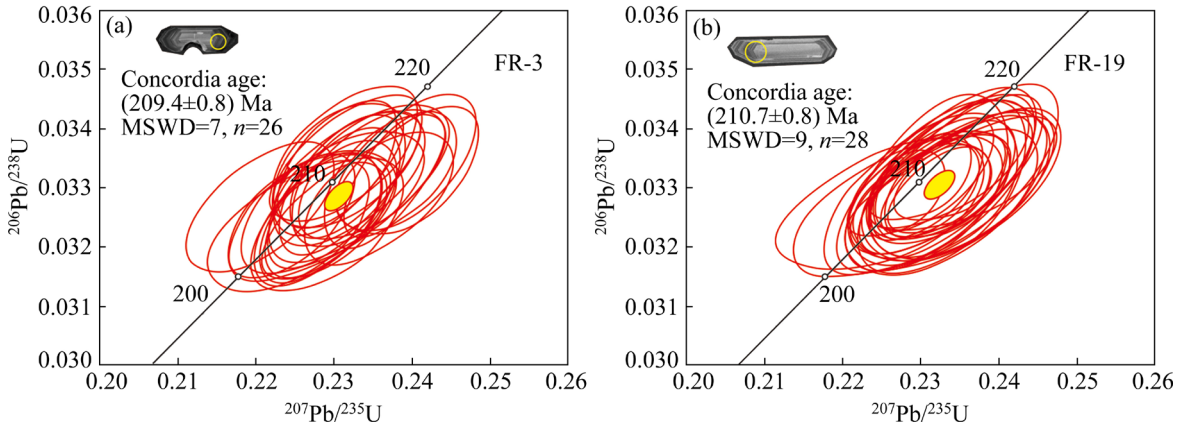


**Fig. 4** Concordia diagrams for zircons collected from Furong pluton (MSWD is mean squared weighted deviation; $n$ is number of samples)

**Table 1** Contents of major oxides for granite samples from Furong pluton (wt.%)

| Oxide | FR-1 | FR-3 | FR-4 | FR-5 | FR-6 | FR-8 | FR-11 | FR-14 | FR-16 | FR-19 |
|---|---|---|---|---|---|---|---|---|---|---|
| $SiO_2$ | 73.9 | 73.3 | 71.4 | 72.9 | 72.5 | 71.3 | 73.1 | 71.7 | 71.9 | 72.4 |
| $TiO_2$ | 0.175 | 0.201 | 0.242 | 0.156 | 0.159 | 0.175 | 0.252 | 0.233 | 0.195 | 0.244 |
| $Al_2O_3$ | 13.6 | 14.1 | 15.1 | 14.4 | 14.8 | 15.2 | 14.0 | 14.9 | 14.9 | 14.7 |
| $Fe_2O_3$(T) | 1.44 | 1.56 | 1.64 | 1.34 | 1.38 | 1.47 | 2.03 | 1.80 | 1.53 | 1.62 |
| MnO | 0.023 | 0.023 | 0.026 | 0.031 | 0.027 | 0.026 | 0.033 | 0.026 | 0.027 | 0.025 |
| MgO | 0.540 | 0.620 | 0.730 | 0.550 | 0.630 | 0.630 | 0.810 | 0.750 | 0.640 | 0.690 |
| CaO | 1.92 | 2.18 | 2.51 | 1.76 | 2.25 | 2.24 | 2.37 | 2.47 | 2.21 | 2.35 |
| $Na_2O$ | 3.04 | 3.21 | 3.52 | 3.44 | 3.60 | 3.45 | 3.23 | 3.61 | 3.43 | 3.66 |
| $K_2O$ | 3.60 | 3.44 | 3.31 | 3.90 | 3.00 | 3.69 | 2.80 | 3.00 | 3.51 | 2.97 |
| $P_2O_5$ | 0.065 | 0.082 | 0.077 | 0.063 | 0.067 | 0.081 | 0.077 | 0.070 | 0.075 | 0.065 |
| *LOI | 0.826 | 0.654 | 1.337 | 0.783 | 1.16 | 1.20 | 1.18 | 0.775 | 1.00 | 1.06 |
| Total | 99.14 | 99.37 | 99.92 | 99.29 | 99.63 | 99.46 | 99.87 | 99.34 | 99.40 | 99.72 |
| A/CNK | 1.09 | 1.08 | 1.08 | 1.10 | 1.12 | 1.10 | 1.10 | 1.09 | 1.10 | 1.08 |

*LOI=Loss on ignition; A/CNK=$w(Al_2O_3)/(w(CaO)+w(Na_2O)+ w(K_2O))$

further ascertain the petrogenesis of the Furong pluton, geochemical data for the Weishan pluton are also referred in the following section.

The Furong granite exhibits relatively high $w(SiO_2)$, $w(K_2O)$ and $w(Na_2O)+w(K_2O)$ contents; low $w(Al_2O_3)$, $w(Fe_2O_3(T))$ and $w(MgO)$ contents. All samples plot within the granite field on the $(w(Na_2O)+w(K_2O))-w(SiO_2)$ (TAS) diagram (Fig. 5). Variable A/CNK ($w(Al_2O_3)/(w(CaO)+w(Na_2O)+w(K_2O))$) ratios for the Furong pluton range from 1.08 to 1.12, indicative of weakly peraluminous signature. The studied pluton displays a moderately differentiation index (D.I.=82−87) and low $w(Mg)$, $w(Fe)$, $w(Ti)$, $w(Ca)$ and $w(P)$ contents, suggesting that the pluton underwent a relatively strong magma differentiation [14].

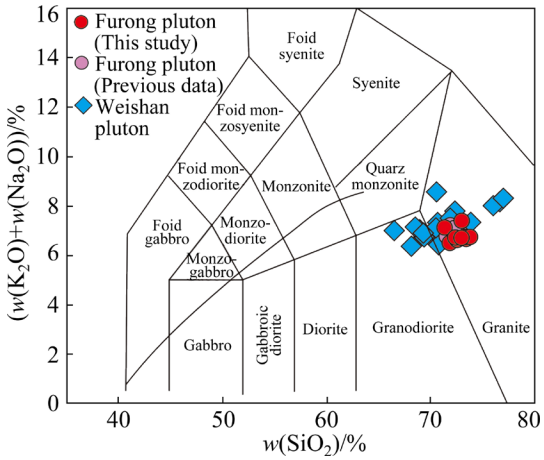


**Fig. 5** TAS diagram of major elements for Furong pluton and Weishan plutons [22] (Previous data for Furong pluton adopted from Ref. [21]; Data for Weishan pluton cited from Refs. [8,20,23,24])

Rare earth element (REE) and trace element data for the Furong pluton are presented in Table 2. The pluton displays moderate REE contents, and the total REE content (∑REE) varies in the range of $(55.3-113.8)\times10^{-6}$ (averaging $79.9\times10^{-6}$) (Table 2). All samples show consistent chondrite-normalized REE patterns (Fig. 6 [25]), and obviously exhibit light rare earth element (LREE) relative enrichment and heavy rare earth element (HREE) relative depletion ($w(La_N)/w(Yb_N)$=17.5−28.8). It is worthwhile to note that, the internal fractionation of LREE ($w(La_N)/w(Sm_N)$=5.0−6.5) is obviously higher than that of HREE ($w(Gd_N)/w(Yb_N)$=2.21−3.61), thus, all samples display steep LREE distribution patterns and relatively flat HREE patterns (Fig. 6). The $\delta_{Eu}$ values change from 0.44 to 0.80, with an average of 0.71, thus the studied pluton exhibits weak negative Eu anomalies, which indicates that there exists the fractional crystallization of feldspar during magma evolution, but the fractional crystallization is relatively weak.

On the primitive mantle-normalized spider diagram (Fig. 7), the Furong pluton is relatively enriched in Th, U, Pb, Nd, Zr and Hf, but is relatively depleted in Ba, Nb, Sr, Eu and Ti. The adjacent Weishan pluton shares similar geochemical characteristics, as shown in Fig. 7.

### 3.3 Sr and Nd isotopic compositions

The Sr and Nd isotopic compositions of the Furong pluton are presented in Table 3. The Furong pluton exhibits the restricted present-day $^{87}Sr/^{86}Sr$ (0.719947−0.723171) and $^{143}Nd/^{144}Nd$ (0.512048−0.512099) values, and its time-calibrated values $(^{87}Sr/^{86}Sr)_i$ range from 0.713582 to 0.714542, and the calculated $\varepsilon_{Nd}(t)$ (deviation of $^{143}Nd/^{144}Nd$ from the standard value) values fall in the range from −9.4 to −8.4 (Table 3). The two-stage Nd model ages ($T_{2DM}$) are calculated at 1.67−1.75 Ga (Table 3).

## 4 Discussion

### 4.1 Emplacement time of granitic plutons

The ages of (209.4±0.8) Ma and (210.7±0.8) Ma obtained for the Furong pluton in this study are consistent with zircon U–Pb ages ((210.8±0.8) Ma and (210.6±1.9) Ma) for the Weishan pluton reported by HU et al [26], and also show good agreement with previously reported dates for the Weishan pluton, including zircon U−Pb ages of (211.0±1.6) Ma and (215.7±1.9) Ma [20] and (204.5±2.8)−(209.2±3.8) Ma [24]. These dates are slightly younger than the emplacement time of other Early Mesozoic in South China (221.7−228.7 Ma) [9,12,14,27]. In spite of these discrepancies, all dates above mentioned fall within the range of the Indosinian period. Therefore, the Late Triassic should be recognized as a critical period for the granitic magmatism in the Furong–Weishan area.

The question whether the Indosinian granites in central Hunan were emplaced during a single geological event or multiple events remains controversial. Based on the dates obtained in this study and other recently published radiometric data of granites in central Hunan, we statistically analyzed the formation time of the early Mesozoic granites in the region (Fig. 8).

**Table 2** Contents of rare earth elements and trace elements for granite samples from Furong pluton ($10^{-6}$)

| Element | FR-1 | FR-3 | FR-4 | FR-5 | FR-6 | FR-8 | FR-11 | FR-14 | FR-16 | FR-19 |
|---|---|---|---|---|---|---|---|---|---|---|
| La | 14.6 | 25.0 | 23.6 | 19.5 | 17.2 | 13.6 | 29.3 | 20.9 | 20.2 | 21.8 |
| Ce | 25.7 | 43.3 | 40.9 | 34.2 | 30.0 | 24.5 | 52.1 | 36.6 | 35.3 | 38.2 |
| Pr | 2.62 | 4.35 | 4.05 | 3.43 | 3.12 | 2.56 | 5.27 | 3.67 | 3.56 | 3.87 |
| Nd | 8.89 | 14.5 | 13.5 | 11.5 | 10.4 | 8.89 | 17.9 | 12.3 | 11.9 | 13.0 |
| Sm | 1.67 | 2.50 | 2.27 | 2.09 | 2.11 | 1.71 | 3.25 | 2.19 | 2.14 | 2.27 |
| Eu | 0.407 | 0.500 | 0.503 | 0.418 | 0.413 | 0.396 | 0.420 | 0.511 | 0.460 | 0.514 |
| Gd | 1.35 | 1.80 | 1.65 | 1.55 | 1.82 | 1.34 | 2.35 | 1.65 | 1.56 | 1.68 |
| Tb | 0.200 | 0.238 | 0.225 | 0.232 | 0.291 | 0.193 | 0.309 | 0.237 | 0.223 | 0.234 |
| Dy | 1.01 | 1.12 | 1.07 | 1.18 | 1.58 | 0.980 | 1.42 | 1.19 | 1.09 | 1.18 |
| Ho | 0.179 | 0.195 | 0.183 | 0.200 | 0.286 | 0.173 | 0.235 | 0.208 | 0.183 | 0.207 |
| Er | 0.477 | 0.499 | 0.457 | 0.523 | 0.750 | 0.456 | 0.574 | 0.534 | 0.465 | 0.538 |
| Tm | 0.071 | 0.072 | 0.067 | 0.080 | 0.108 | 0.068 | 0.085 | 0.079 | 0.070 | 0.082 |
| Yb | 0.443 | 0.448 | 0.421 | 0.509 | 0.664 | 0.421 | 0.525 | 0.489 | 0.435 | 0.530 |
| Lu | 0.063 | 0.065 | 0.061 | 0.073 | 0.090 | 0.060 | 0.077 | 0.070 | 0.063 | 0.076 |
| Y | 5.54 | 5.83 | 5.50 | 6.25 | 8.73 | 5.29 | 7.08 | 6.29 | 5.62 | 6.41 |
| Sc | 3.46 | 3.65 | 3.87 | 3.54 | 3.39 | 2.99 | 4.53 | 4.48 | 3.75 | 4.35 |
| Rb | 194 | 185 | 186 | 269 | 161 | 165 | 168 | 182 | 204 | 198 |
| Ba | 335 | 591 | 485 | 649 | 257 | 412 | 334 | 435 | 557 | 457 |
| Th | 9.12 | 15.2 | 12.4 | 11.8 | 11.7 | 9.34 | 20.7 | 12.5 | 11.7 | 13.4 |
| U | 2.57 | 3.51 | 8.13 | 6.01 | 18.1 | 4.50 | 4.54 | 10.2 | 3.48 | 6.47 |
| Ta | 0.976 | 0.846 | 0.833 | 2.05 | 0.973 | 0.892 | 1.11 | 0.904 | 1.54 | 1.35 |
| Nb | 6.04 | 6.08 | 5.89 | 9.30 | 7.48 | 5.32 | 8.03 | 6.85 | 7.79 | 7.37 |
| Pb | 42.8 | 40.0 | 37.8 | 43.0 | 44.5 | 38.8 | 33.9 | 39.3 | 41.6 | 41.0 |
| Sr | 182 | 221 | 258 | 187 | 192 | 173 | 187 | 252 | 208 | 246 |
| Zr | 86.8 | 110 | 110 | 81.4 | 90.8 | 67.1 | 112 | 107 | 93.0 | 114 |
| Hf | 2.46 | 2.92 | 2.93 | 2.58 | 2.62 | 1.90 | 3.17 | 2.91 | 2.66 | 3.22 |
| W | 0.383 | 0.343 | 0.987 | 0.555 | 0.322 | 0.744 | 0.663 | 0.289 | 0.703 | 0.310 |
| $w(\sum\text{REE})$ | 57.7 | 94.6 | 89.0 | 75.5 | 68.8 | 55.3 | 113.8 | 80.6 | 77.7 | 84.2 |
| $\delta_{Eu}$ | 0.80 | 0.69 | 0.76 | 0.68 | 0.63 | 0.77 | 0.44 | 0.79 | 0.74 | 0.77 |
| $w(La)_N/w(Sm)_N$ | 5.5 | 6.3 | 6.5 | 5.9 | 5.1 | 5.0 | 5. 7 | 6.0 | 5.9 | 6.0 |
| $w(Gd)_N/w(Yb)_N$ | 2.5 | 3.2 | 3.2 | 2.5 | 2.2 | 2.6 | 3.6 | 2.7 | 2. 9 | 2. 6 |
| $T_{Zr}$/°C | 743 | 760 | 757 | 736 | 746 | 719 | 763 | 756 | 746 | 761 |

$T_{Zr}$ is the whole-rock Zr saturation temperature

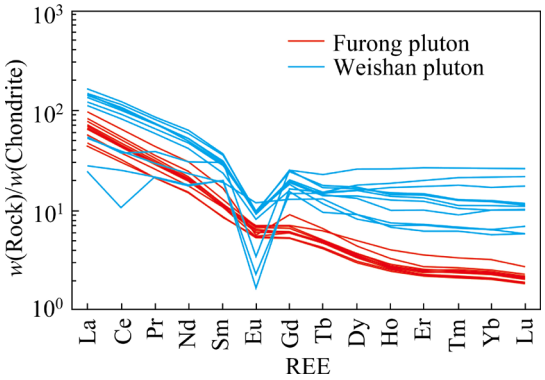


**Fig. 6** Chondrite-normalized REE patterns for Furong and Weishan plutons (The normalized values cited from Ref. [25]; data for Weishan pluton adopted from Refs. [8,20])

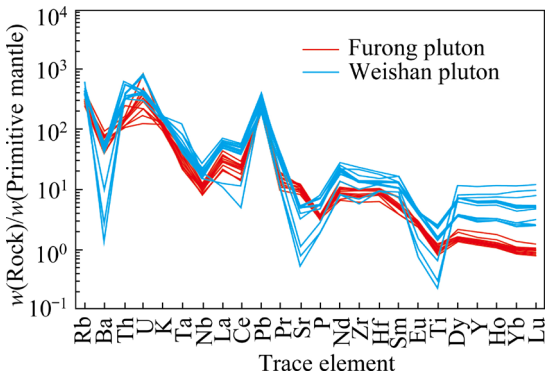


**Fig. 7** Primitive mantle-normalized spider diagram for Furong and Weishan plutons (The normalized values cited from Ref. [25]; Data for Weishan pluton adopted from Refs. [8,20])

**Table 3** Rb−Sr and Sm−Nd isotopic compositions of granite samples from Furong pluton

| Sample | $^{87}Rb/^{86}Sr$ | $^{87}Sr/^{86}Sr$ | $^{147}Sm/^{144}Nd$ | $^{143}Nd/^{144}Nd$ | $(^{87}Sr/^{86}Sr)_i$ | $(^{143}Nd/^{144}Nd)_i$ | $\varepsilon_{Nd}(t=210\ Ma)$ | $t_{2DM}$/Ga |
|---|---|---|---|---|---|---|---|---|
| FR-1 | 3.086519 | 0.723171 | 0.113568 | 0.512076 | 0.713953 | 0.511920 | −8.7 | 1.70 |
| FR-3 | 2.423919 | 0.721115 | 0.104234 | 0.512062 | 0.713876 | 0.511918 | −8.8 | 1.70 |
| FR-4 | 2.087526 | 0.719947 | 0.101656 | 0.512071 | 0.713712 | 0.511931 | −8.5 | 1.68 |
| FR-5 | 4.165328 | 0.726022 | 0.109872 | 0.512084 | 0.713582 | 0.511933 | −8.5 | 1.68 |
| FR-6 | 2.428081 | 0.721688 | 0.122656 | 0.512099 | 0.714437 | 0.511931 | −8.5 | 1.68 |
| FR-8 | 2.761699 | 0.722789 | 0.116288 | 0.512048 | 0.714542 | 0.511888 | −9.4 | 1.75 |
| FR-11 | 2.601395 | 0.721926 | 0.109766 | 0.512066 | 0.714157 | 0.511916 | −8.8 | 1.71 |
| FR-14 | 2.091267 | 0.720105 | 0.107641 | 0.512075 | 0.713859 | 0.511927 | −8.6 | 1.69 |
| FR-16 | 2.839915 | 0.722799 | 0.108719 | 0.512074 | 0.714318 | 0.511924 | −8.7 | 1.69 |
| FR-19 | 2.330605 | 0.720818 | 0.105565 | 0.512084 | 0.713857 | 0.511939 | −8.4 | 1.67 |

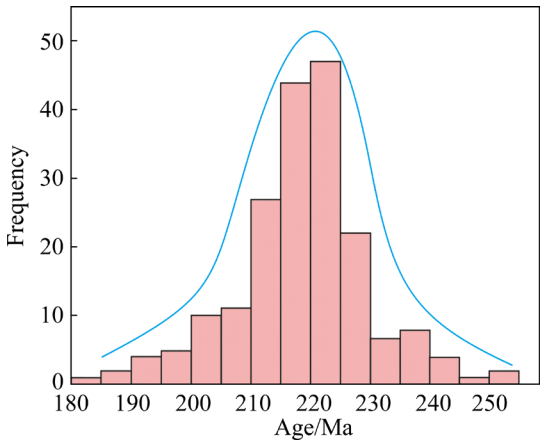


**Fig. 8** Histogram of emplacement time for Indosinian granites in central Hunan

As shown in Fig. 8, all dates ($n$=181) for the Mesozoic granites in central Hunan fall in a relatively narrow range of 180−255 Ma, mostly clustering at an interval of 210−230 Ma. Some researchers have claimed that there existed two different kinds of Indosinian granites in central Hunan [8,14,23]: the early granite formed at 225−240 Ma, and the late granite was emplaced at 200−225 Ma. However, the emplacement time exhibits a good normal distribution (Fig. 8), which seems to rule out the possibility of two independent magmatic events happened in the studied region, thus, all Indosinian granites in the region are likely to be formed during a continuous but prolonged magmatic event.

### 4.2 Classification of granitic rocks

According to field survey, mineralogy, geochemistry and isotopic data, granites can be classified into I-type, S-type, A-type and M-type [28,29]. A-type granites typically display high $w(SiO_2)$, $w(Na_2O)+w(K_2O)$, $w(Zr)$, $w(Nb)$ and $w(Fe_2O_3(T))/w(MgO)$ values, low $w(CaO)$ and $w(Sr)$ contents, significantly negative Eu anomaly, and high magma temperatures. Obviously, the geochemical characteristics of the Furong pluton are different from those of A-type granites. The Zr contents of the Furong pluton vary in the range of $(67.1-114)\times10^{-6}$, significantly less than that of A-type granite ($250\times10^{-6}$). In addition, its weak negative Eu anomaly ($\delta_{Eu}$=0.44−0.80) and lower zircon-saturation temperatures (719−763 °C) also preclude the possibility that the studied pluton belongs to A-type granite.

In the $w(Fe_2O_3(T))-w(MgO)-w(Al_2O_3)$ ternary diagram, all samples in this study fall into the field of S-type granite (Fig. 9 [30]), indicating the Furong pluton should be classified into the S-type granite. Its high $w(SiO_2)$ and $w(K_2O)$ contents, low $w(P_2O_5)$ content, Rb, Th, U and Pb enrichment, and Ba, Sr and Eu depletion, also indicate that the pluton is a typical one of S-type granites. Moreover, some peraluminous minerals, including white mica, tourmaline and even garnet, can be observed in some samples in this study, providing a more convincing evidence for its S-type origin.

### 4.3 Nature of source rocks and formation mechanism

There are two distinct kinds of mechanisms for the formation of granitic magma, including re-melting of ancient continental and differentiation of basaltic magma [31]. Some trace elements and isotopes can be used to discriminate the above formation mechanisms [31].

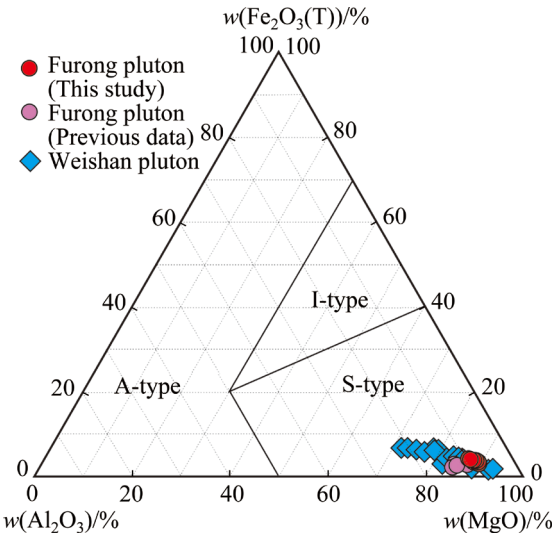


**Fig. 9** Ternary diagram of $w(Fe_2O_3(T))$−$w(Al_2O_3)$−$w$(MgO) for Furong and Weishan plutons [30] (Previous data for Furong pluton adopted from Ref. [21]; Data for Weishan pluton cited from Refs. [8,20,23,24])

The $(^{87}Sr/^{86}Sr)_i$ values of the Furong pluton vary in the range of 0.713582−0.714542, significantly higher than that of mantle (0.704256; $t$=210 Ma), and even higher than the average value of the continental crust, ruling out the possibility of those basaltic rocks in mantle as the major source rocks. The Sr and Nd isotopic compositions of the studied plutons are similar to those of the Yangtze upper continental crust (Fig. 10(a)). The Nd isotopic characteristics of these granites are consistent with the Proterozoic crustal evolutionary domain of South China (Fig. 10(b)), thus the continental materials are mainly responsible for the pluton formation. The $w$(Nb)/$w$(Ta) ratios of the studied pluton fall within the range of 4.5−7.7, significantly less than the average value of continental crust (11−17.5), indicating that the partial melting of the continental crust is responsible for the formation of the studied pluton [14,31]. As shown in Table 3, the pluton exhibits relatively low $\varepsilon_{Nd}(t)$ values (from −8.4 to −9.4), revealing that the granite is likely to be derived from either partial melting of metasedimentary rocks or partial melting of more juvenile crustal materials. Many previous researches also confirmed that the re-melting of crustal materials is the most important mechanism for the formation of those tungsten-associated granites [3,14,18]. The two-stage Nd model ages ($t_{2DM}$) of 1.67−1.75 Ga (Table 3) further revealed that the source rocks of the studied plutons are of the Paleoproterozoic sedimentary origin. However, those positive Pb anomalies in the spider diagram (Fig. 7), as well as those small $w$(Y)/$w$(Nb) ratios (0.67−1.17, averaging 0.90), also revealed that the juvenile crustal materials were likely to be involved in the initial magma [31].

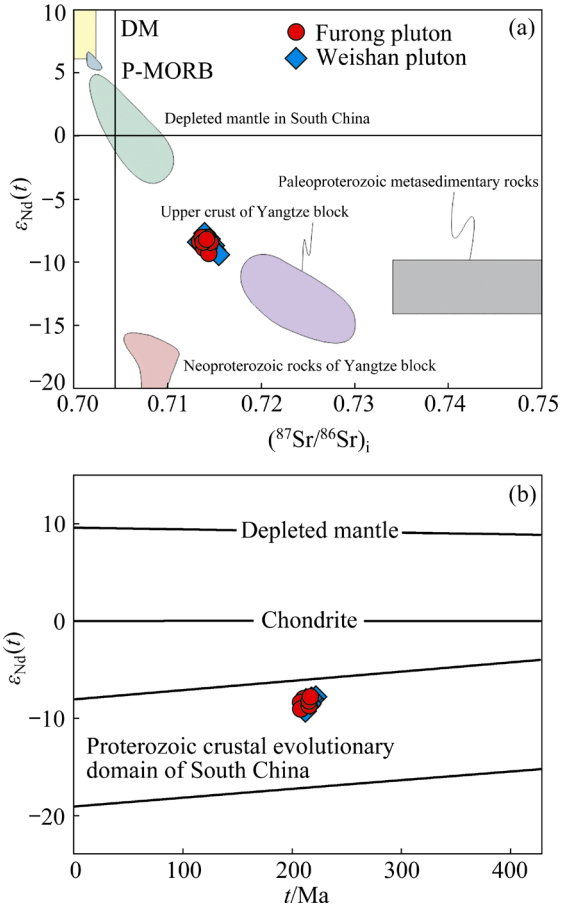


**Fig. 10** Plots of $(^{87}Sr/^{86}Sr)_i$ versus $\varepsilon_{Nd}(t)$ (a) and age ($t$) versus $\varepsilon_{Nd}(t)$ (b) of granite samples from Furong and Weishan plutons (Modified after Ref. [32]; Data for Weishan pluton adopted from Refs. [8,20,23])

Although that the formation mechanism is dominated by the re-melting of ancient continental crust, the fractional crystallization also played certain role during the magma emplacement. For example, the fractional crystallization of plagioclase is indicative of those negative Eu anomaly in Fig. 6, together with the obvious Sr and Ba depletion in Fig. 7. The significant Nb, Ta and Ti depletion in Fig. 7 indicates that there is the fractional crystallization of Ti-rich minerals, such as ilmenite and rutile. The $P_2O_5$ depletion reveals the existence of apatite fractional crystallization during the formation of the Furong pluton.

As mentioned above, the Furong pluton contains abundant tungsten resource (Fig. 2).

Previous studies showed that the basement strata in South China were rich in tungsten, tin (Sn) and other ore-forming metals [6,15,33], and muscovite and biotite were believed to be the most important tungsten-bearing minerals in the source rocks [34]. The zircon-saturation temperatures of the studied pluton change from 719 to 763 °C (averaging 749 °C) (Table 2), which coincide well with the temperature of the muscovite dehydration melting (~750 °C) and are obviously less than that of the biotite dehydration melting (~800 °C) [6,33]. During the partial melting controlled by muscovite dehydration, the element W will be released and transferred into the melt, while Sn still remains in the residue [6]. Therefore, it can be concluded that the Furong pluton was mainly generated via the muscovite dehydration melting rather than the biotite dehydration melting. The silicate magma resulted from the muscovite dehydration melting exhibits higher Pb and Al concentrations and lower Ti concentrations [33], and it is true for the studied pluton.

### 4.4 Geodynamic implications

The Jiangnan Orogen is located in the amalgamation zone of the Yangtze block and the Cathaysia block in South China, and it has experienced at least three tectonic events since the Phanerozoic [14,35]. From the Ordovician to the Devonian, South China experienced intracontinental orogeny, forming some extensive NNE-trending structures in South China [36]. The South China Plate was in an active stage from the Late Permian to the Early Triassic, including collision with the North China Plate along the Qinling−Dabie orogenic belt to the north and collision with the Indochina Plate to the west [35]. This activity peaked at 258−243 Ma, forming the infancy of South China Plate [8]. From the Early Indosinian (243−225 Ma) to the Late Indosinian (225−206 Ma), South China Plate experienced intraplate orogeny and transformed from a collision compression environment to a post-collision extension environment [8,24,27]. On the tectonic discrimination diagrams of $w$(Y)+$w$(Nb) versus $w$(Rb) (Fig. 11(a)) and $w$(Rb)/30−$w$(Hf)−3$w$(Ta) (Fig. 11(b)) of Furong pluton, all samples in this study fall in the syn-collision and post-collision fields. As stated above, the emplacement time of the Furong pluton is determined at ~210 Ma, which is 14−20 Ma younger than the peak time of the high-grade metamorphism in the Qinling–Dabie collision zone (230−226 Ma) [14,35] and 15−33 Ma less than the time of the Early Indosinian collision orogeny (243−225 Ma) in South China. Therefore, the Furong pluton probably formed as a result of the crustal extension and thinning after the intraplate collision. All most the emplacement time for other Indosinian granites in central Hunan was less than 225 Ma (Fig. 8), thus these granites in central Hunan also formed under the tectonic background of post-collision [12,14,27].

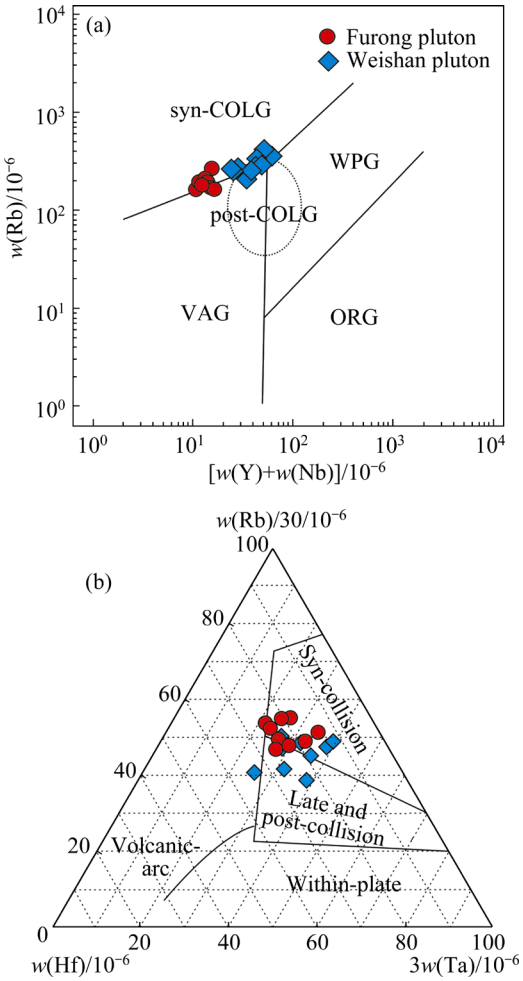


**Fig. 11** Tectonic discrimination diagrams for Furong pluton: (a) $w$(Y)+$w$(Nb)–$w$(Rb) [37]; (b) $w$(Rb)/30–$w$(Hf)−3$w$(Ta) [38] (Data for Weishan pluton adopted from Ref. [8,20])

### 4.5 Relationship between pluton and tungsten mineralization

Tungsten is a clean energy source and an indispensable strategic metal in the information industry, national defense industry, and other fields [39]. Tungsten mineralization researches have been the focus of international mineral deposit

researches in recent years [2,5,12,40]. South China is the largest tungsten mineralization concentrated region throughout the world, and the proven tungsten reserves of this region account for more than 50% of the global total reserves [2,6,7]. These tungsten deposits are closely related to the Late Mesozoic highly-differentiated granites, and usually occur in the interior of granites or in the contact zone between granites and wallrocks [2,11,27].

The moderately-differentiated Furong pluton hosts a medium-sized tungsten deposit dominated by scheelite mineralization. However, the absence of suitable minerals in ores for the conventional dating method precluded the possibility of direct determination on the metallogenic age for the Furong deposit. Luckily, we recently obtained the Ar–Ar ages of 210 Ma and 209 Ma for muscovite collected from two greisen samples in the adjacent Situpu mining district (unpublished data). Both the Ar–Ar ages for tungsten mineralization coincide well with the emplacement time of the Furong and Weishan plutons. Therefore, it can be concluded that the tungsten mineralization in the Furong mining district is contemporaneous with the emplacement time of the Furong pluton.

In contrast to the tungsten mineralization associated with Late Mesozoic highly-differentiated granite in the Nanling Range, those tungsten deposits associated with moderately-differentiated in central Hunan were formed in the Early Mesozoic, except for the Yangjiashan W−Cu deposit [41]. As mentioned above, some important Indosinian tungsten deposits include the Muguayuan tungsten deposit [12], Baojinshan W−Au deposit [16], Xingfengshan W−Au deposit [19], Situpu tungsten deposit [26], Zanshi tungsten deposit [27], Darongxi tungsten deposit [42] and Furong tungsten deposit in this study. The mineralization ages of these tungsten deposits are basically consistent with the intrusion time of the surrounding granites. According to the following evidences, the Indosinian tungsten mineralization is closely related to the Early Mesozoic granites in central Hunan. Firstly, the basement strata in South China are rich in tungsten and other metallogenic metals [6,33]. Secondly, strong intraplate collisions and the suitable partial-melting temperature are responsible for the effective release of tungsten from the source rocks into the original magma [6,14,33]. Finally, the magma rich in water and volatile is conducive to further enrichment of tungsten during the magma evolution [3,30,33,42]. The extensive tungsten mineralization in the Early Mesozoic in central Hunan resulted from igneous activity [10,14].

Tungsten is a lithophilic element in the continental crust and usually acts as an incompatible element. It usually tends to accumulate in residual melt during the magma crystallization; therefore, it is generally believed that those highly-differentiated granites are conducive to tungsten mineralization [33,34]. The Late Mesozoic tungsten-bearing granite in the Nanling Range in China is a typical example. However, a few recent studies have shown that some granites with moderately-differentiation can also form world-class tungsten deposits such as Cantung and Mactung deposits in Northern Cordillera [43,44]. The Indosinian granites in central Hunan share similar petrological and geochemical characteristics with those tungsten-bearing deposits in Northern Cordillera, and also display some significant mineralization potential for tungsten resources; thus, the Indosinian tungsten mineralization in the region is of great economic significance, and its resource potential was previously underestimated.

## 5 Conclusions

(1) The granite hosted tungsten mineralization in the Furong mining district belongs to the S-type granite. The emplacement time of the pluton is precisely determined to be ~210 Ma. The emplacement time of the Indosinian granites was strictly restricted in the range of 180–255 Ma, and all Indosinian granites in the middle section of Jiangnan Orogen were formed during a continuous but prolonged magmatic event.

(2) The partial melting of Paleoproterozoic metasedimentary rocks through the muscovite-dehydration is mainly responsible for the formation of the studied pluton, and the granite may have been derived from either partial melting of metasedimentary rocks or partial melting of more juvenile crustal materials. The granite emplacement in the studied region resulted from the crustal extension and thinning of after intraplate collision and compression.

(3) Tungsten mineralization and the moderately differentiated granites in central Hunan exhibit a close spatial, temporal, and genetic relation-ships. The significance of the Indosinian granites

and its related mineralization were previously underestimated, and the further prospecting of tungsten mineralization within and around the Early Mesozoic granite in central Hunan is urgently needed.

## CRediT authorship contribution statement

**Jian-xiong DU**: Geological survey, Conceptualization, Writing − Original draft; **Jian-tang PENG**: Geological survey, Writing − Review & editing, Supervision, Funding acquisition; **A-xiang HU**: Geological survey, Methodology, Data analysis and interpretation, Writing − Review & editing, Funding acquisition; **Ta-gen DAI**: Writing − Review & editing, Supervision; **Meng-ying SUO**: Geological survey, Data analysis and interpretation; **Li-chao XIAHOU**: Geological survey, Data interpretation.

## Declaration of competing interest

The authors declare that they have no known competing financial interests or personal relationships that could have appeared to influence the work reported in this paper.

## Acknowledgments

This work was financially supported by the Natural Key Research and Development Program of China (No. 2023YFC2906801), the National Natural Science Foundation of China (No. 42102073), and the Open Protect Fund of State Key Laboratory of Critical Mineral Research and Exploration, China (No. 202308). We are grateful for Prof. Wen-hua HE from Hunan Institute of Geological Research for his help during our field investigation.

## References

[1] ZHANG Xiao-yu, ZHAO Kui-dong, CHENG Kai-de, ZHANG Wei, LI Qian, JIANG Shao-yong. W-rich zircons from the granite in the Hukeng tungsten deposit, South China: Genesis and exploration significance [J]. Ore Geology Reviews, 2024, 169: 106103.

[2] NI Pei, PAN Jun-yi, HAN Liang, CUI Jian-ming, GAO Yan, FAN Ming-sen, LI Wen-sheng, CHI Zhe, ZHANG Kai-han, CHENG Zhi-lin, LIU Yu-pei. Tungsten and tin deposits in South China: Temporal and spatial distribution, metallogenic models and prospecting directions [J]. Ore Geology Reviews, 2023, 157: 105453.

[3] MA Xing-hua, WANG Hong-hui, LEHMANN B, GUO Chun-li, MAO Jing-wen. Control of magmatic halogen composition and redox state on the zonation of metal mineralization across active continental margins: Perspectives from the world-class South China metallogenic province [J]. Chemical Geology, 2024, 669: 122363.

[4] ZHANG Wei, JIANG Shao-yong, OUYANG Yong-peng, ZHANG Di. Geochronology and textural and compositional complexity of apatite from the mineralization-related granites in the world-class Zhuxi W−Cu skarn deposit: A record of magma evolution and W enrichment in the magmatic system [J]. Ore Geology Reviews, 2021, 128: 103885.

[5] ZHANG Feng, GUO Feng, ZHANG Xiao-bing, ZHAO Liang, HUA Wei-cheng, HUANG Xin, TIAN Xu-feng. Multiple-pulse magmatic intrusion and fluid metasomatism in Mesozoic Qianlishan rare metal granite, South China: Records from apatite geochemistry [J]. Lithos, 2024, 474/475: 107580.

[6] YUAN Shun-da, WILLIAMS-JONES A E, ROMER R L, ZHAO Pan-lao, MAO Jing-wen. Protolith-related thermal controls on the decoupling of Sn and W in Sn−W metallogenic provinces: Insights from the Nanling Region, China [J]. Economic Geology, 2019, 114: 1005−1012.

[7] ZHU Da-peng, LI Huan, JIANG Wei-cheng, WANG Chong, HU Xiao-jun, KONG Hua. Ore-forming environment of Pb−Zn mineralization related to granite porphyry at Huangshaping skarn deposit, Nanling Range, South China [J]. Transactions of Nonferrous Metals Society of China, 2022, 32: 3015−3035.

[8] WANG Yue-jun, FAN Wei-ming, SUN Min, LIANG Xin-quan, ZHANG Yan-hua, PENG Tou-ping. Geochronological, geochemical and geothermal constraints on petrogenesis of the Indosinian peraluminous granites in the South China Block: A case study in the Hunan Province [J]. Lithos, 2007, 96: 475−502.

[9] WU Jing, LIANG Hua-ying, HUANG Wen-ting, WANG Chun-long, SUN Wei-dong, SUN Ya-li, LI Jing, MO Ji-hai, WANG Xiu-zhang. Indosinian isotope ages of plutons and deposits in southwestern Miaoershan—Yuechengling, Northeastern Guangxi and implications on Indosinian mineralization in South China [J]. China Science Bulletin, 2012, 57(13): 1024−1035. (in Chinese)

[10] ZHANG Zhi-yuan, XIE Gui-qing, OLIN P. Tungsten mineralization in the Caojiaba tungsten deposit, Southern China: Constraints from scheelite in-situ trace elements and Sr isotope evidence [J]. Ore Geology Reviews, 2023, 158: 105496.

[11] LIU Min, ZHAO Pan-lao, HONG Wei, YUAN Shun-da. Assessing the W−Sn ore formation potential of large granite batholiths: Insights from zircon U−Pb and muscovite Ar−Ar geochronology of the Tianmuchong W–Sn deposit in the Nanling region, South China [J]. Ore Geology Reviews, 2024, 174: 106311.

[12] LI Xiao-yu, LU Jian-jun, ZHANG Rong-qing, GAO Jian-feng, WU Jin-wei. Magma evolution leading to veinlet-disseminated tungsten mineralization at the Muguayuan deposit: In-situ analysis of igneous minerals [J]. Ore Geology Reviews, 2021, 138: 104406.

[13] DAI Qian-wei, DUAN Dan, LIU Biao, WU Qian-hong, YAN Jia-bin, KONG Hua, CHEN She-fa, ZONG Qi, TANG Yu-yu. Deep exploration of W−Sn and Cu polymetallic deposits in middle Qin–Hang metallogenic belt, South China [J]. Transactions of Nonferrous Metals Society of China, 2023, 33: 231−253.

[14] DU Yun, LU You-yue, ZHANG Zun-zun, FU Jian-ming, YANG Xiao-yong, ZHAO Zhuang, QIN Zheng-wei, CHEN Jian-feng, XIAO Rong, LI Jian-feng, CHEN Xi-qing, ZHENG Zheng-fu, ZENG Zhi-fang, XIAO Dong-gui, DAI Ping-yun, MA Li-yan. Indosinian magmatism and mineralization in the Banjiaoyuan tin deposit, middle Nanling Range, South China: Constraints from zircon and cassiterite U−Pb ages, geochemistry and Sr−Nd−Hf isotopic compositions [J]. Ore Geology Reviews, 2022, 151: 105190.

[15] HU Xiao-jun, LI Huan, ALGEO T J, LIU Biao, KANG Fan, XIE Yi-ming, ZHU Da-peng. Differentiating Triassic W−Sn ore-bearing and ore-free plutons in the Xitian Ore Field (South China) using apatite geochemistry [J]. Journal of Geochemical Exploration, 2025, 268: 107628.

[16] PENG Jian-tang, WANG Chuan, LI Yu-kun, HU A-xiang, LU Yu-long, CHEN Xian-jia. Geochemical characteristics and Sm−Nd geochronology of scheelite in the Baojinshan ore district, central Hunan [J]. Acta Petrologica Sinica, 2021, 37(3): 665−682. (in Chinese)

[17] LIANG Yong-ke, ZHAO Jie, WANG De-gong. Geological features and prospecting indicators of Furong scheelite mining area in Hunan [J]. Guizhou Geology, 2017, 34(4): 255−261. (in Chinese)

[18] WANG Xiao-lei, ZHOU Jin-cheng, CHEN Xin, ZHANG Feng-feng, SUN Zi-ming. Formation and evolution of the Jiangnan Orogen [J]. Bulletin of Mineralogy, Petrology and Geochemistry, 2017, 36(5): 714−735, 696. (in Chinese)

[19] LÜ Yuan-jun, PENG Jian-tang, CAI Ya-fei. Geochemical characteristics, U−Pb dating of hydrothermal titanite from the Xingfengshan tungsten deposit in Hunan Province and their geological significance [J]. Acta Petrologica Sinica, 2021, 37(3): 830−846. (in Chinese)

[20] DING Xing, CHEN Pei-rong, CHEN Wei-feng, HUANG Hong-ye, ZHOU Xin-min. Single zircon LA-ICPMS U−Pb dating of Weishan granite (Hunan, South China) and its petrogenetic significance [J]. Science in China (Series D): Earth Sciences, 2006, 49(8): 816−827.

[21] Geological Survey Institute of Hunan Province. The regional geology of China, Hunan Province [M]. Beijing: Geology Press, 2017. (in Chinese)

[22] ERIC A K M. Naming materials in the magma/igneous rock system [J]. Earth-Science Reviews, 1994, 37(3/4): 215−224.

[23] WANG Yue-jun, FAN Wei-ming, LIANG Xin-quan, PENG Tou-ping, SHI Yu-ruo. SHRIMP zircon U–Pb geochronology of Indosinian granites in Hunan Province and its petrogenetic implications [J]. Chinese Science Bulletin, 2005, 50(13): 1395−1403. (in Chinese)

[24] CHEN Wei-feng, CHEN Pei-rong, HUANG Hong-ye, DING Xing, SUN Tao. Chronological and geochemical studies of granite and enclave in Baimashan pluton, Hunan, South China [J]. Science in China (Series D): Earth Sciences, 2007, 50(11): 1606−1627.

[25] SUN M D. Magmatism in the ocean basins [M]. London: Geological Society, 1989.

[26] HU A-xiang, PENG Jian-tang, SUO Meng-ying, XIAHOU Li-chao. Geochronology of the Situpu tungsten deposit in Hunan and its significance for regional metallogensis [J]. Acta Pertrologica Sinica, 2025, 41(6): 1960−1976. (in Chinese)

[27] YU Yu-shuai, ZHOU Yun, DAI Ping-yun, XIE Fei, BAO Bo, LIU Chong-peng. Triassic tungsten mineralization in Nanling metallogenic belt: A case study of the Zanshi tungsten deposit in the Yajiangqiao area, eastern Hunan Province, China [J]. Ore Geology Reviews, 2022, 142: 104710.

[28] CHAPPELL B W, WHITE A J R. Two contrasting granite types [J]. Pacific Geology, 1974, 8: 173−174.

[29] LIU Bo, HAN Bao-fu, REN Rong, ZHENG Bo, CHEN Jia-fu. Late Carboniferous to Early Permian adakitic rocks and fractionated I-type granites in the southern West Junggar terrane, NW China: Implications for the final closure of the Junggar–Balkhash Ocean [J]. Geological Journal, 2020, 55(3):1728−1749.

[30] ABDEL-RAHAMN A F M. Nature of biotites from alkaline, calc-alkaline, and peraluminous magmas[J]. Journal of Petrology, 1994, 35(2): 525−541.

[31] ZHENG Yong-fei, GAO Peng. The production of granitic magmas through crustal anatexis at convergent plate boundaries [J]. Lithos, 2021, 402/403: 106232.

[32] SUN Tao, ZHOU Xin-min, CHEN Pei-rong, LI Hui-min, ZHOU Hong-ying, WANG Zhi-cheng, SHEN Wei-zhou. Strongly peraluminous granites of Mesozoic in Eastern Nanling Range, Southern China: Petrogenesis and implications for tectonics [J]. Science in China (Series D): Earth Sciences, 2005, 48(2): 165−174.

[33] ZHAO Pan-lao, YUAN Shun-da, WILLIAMS-JONES A E, ROMER R L, YAN Chen, SONG Shi-wei, MAO Jing-wen. Temporal separation of W and Sn mineralization by temperature–controlled incongruent melting of a single protolith: Evidence from the Wangxianling area, Nanling Region, South China [J]. Economic Geology, 2022, 117(3): 667−682.

[34] YUAN Shun-da, ZHAO Pan-lao, LIU Min. Some problems involving in petrogenesis and metallogenesis of granite-related tin deposits [J]. Mineral Deposits, 2020, 39(4): 607−618. (in Chinese)

[35] ZHAO Lei, ZHAI Ming-guo, ZHOU Xi-wen. Early Precambrian basement components of the Cathaysia Block in South China exhumed by Phanerozoic orogenic events [J]. Precambrian Research, 2023, 398: 107218.

[36] SHU Liang-shu, YAO Jin-long, WANG Bo, FAURE M, CHARVET J, CHEN Yan. Neoproterozoic plate tectonic process and Phanerozoic geodynamic evolution of the South China Block [J]. Earth-Science Reviews, 2021, 216: 103596.

[37] PEARCE J A, HARRIS N B W, TINDLE A G. Trace element discrimination diagrams for the tectonic interpretation of granitic rocks [J]. Journal of Petrology, 1984, 25: 956−983.

[38] HARRIS N B W, PEARCE J A, TINDLE A G. Geochemical characteristics of collision-zone magmatism [J]. Geological Society, London, Special Publications, 1986, 19: 67−81.

[39] WANG Xu, QIN Wen-qing, JIAO Fen, DONG Liu-yang, GUO Jian-gen, ZHANG Jian, YANG Cong-ren. Review of tungsten resource reserves, tungsten concentrate production and tungsten beneficiation technology in China [J]. Transactions of Nonferrous Metals Society of China, 2022, 32(7): 2318−2338.

[40] CHENG Yong-sheng. Petrogenesis of skarn in Shizhuyuan W-polymetallic deposit, southern Hunan, China: Constraints

from petrology, mineralogy and geochemistry [J]. Transactions of Nonferrous Metals Society of China, 2016, 26: 1676−1687.

[41] XIE Gui-qing, MAO Jing-wen, LI Wei, FU Bin, ZHANG Zhi-yuan. Granite–related Yangjiashan tungsten deposit, southern China [J]. Mineralium Deposita, 2019, 54: 67−80.

[42] SUO Meng-ying, PENG Jian-tang, HU A-xiang, XIAHOU Li-chao, DENG Si-qi. The magma properties of the Indosinian Dashenshan W-bearing granite in Hunan province and their constraints on tungsten mineralization: Evidences from zircon and apatite [J]. Acta Petrologica Sinica, 2025, 41(6): 2017−2033. (in Chinese)

[43] ELONGO V, LECUMBERRI-SANCHEZ P, LEGROS H, FALCK H, ADLAKHA E, ROY-GARAND A. Paragenetic constraints on the Cantung, Mactung and Lened tungsten skarn deposits, Canada: Implications for grade distribution [J]. Ore Geology Reviews, 2020, 125: 103677.

[44] RASMUSSEN K L, FALCK H, ELONGO V, REIMINK J, LUO Y, PEARSON D G, OOTES L, CREASER R A, LECUMBERRI-SANCHEZ P. The source of tungsten-associated magmas in the northern Canadian Cordillera and implications for the basement [J]. Geology, 2023, 51: 657−662.

# 湘中早中生代芙蓉岩体岩石成因及其与钨成矿的关系

杜建雄[1]，彭建堂[2]，胡阿香[2,3]，戴塔根[4]，索梦颖[2]，夏侯立超[4]

1. 贵州财经大学 管理科学与工程学院，贵阳 550025；
2. 中国科学院 地球化学研究所 关键矿产成矿与预测全国重点实验室，贵阳 550081；
3. 湖南城市学院 土木工程学院，益阳 413000；
4. 中南大学 地球科学与信息物理学院，长沙 410083

**摘　要：**芙蓉岩体位于湖南省中部，该岩体内部和周边发育着较多具有重要经济价值的钨矿脉，但对其岩石成因及其相关钨矿的研究很少。本研究采用 U−Pb 定年、岩石学和地球化学手段，查明了芙蓉岩体的侵位时代、岩石类型、源区性质、形成机制及动力学过程。结果表明，芙蓉岩体形成于~210 Ma，属于中等分异的 S 型花岗岩；结合区域构造背景推测其形成于华南板块碰撞挤压后的地壳伸展减薄环境。结果还显示，湘中钨化矿与印支期花岗岩具有密切的时间、空间和成因联系，急需对该区域乃至华南印支期花岗岩内部和周边的钨矿床开展进一步找矿工作。

**关键词：**锆石 U−Pb 定年；印支期；钨矿化；芙蓉岩体；华南

**(Edited by Wei-ping CHEN)**